Design and Performance Optimization of an Inductive Power Transfer Converter for Enhanced Electric Scooter Micromobility Charging

Bilel Touaiti[1,2,3], Yassine Trabelsi[1,2], Hechmi Ben azza[1,2]

[1]Université de Tunis, Ecole Nationale Supérieure d'Ingénieurs de Tunis (ENSIT)
[2]Laboratoire de l'Ingénierie des Systèmes Industriels et des Energies Renouvelables (LISIER).
5 avenue Taha Hussein, BP 56, Montfleury, 1008 Tunis, Tunisie.
[3]Université de Kairouan, Institut Supérieur des Sciences Appliquées et Technologies de Kasserine, Campus universitaire de Kasserine BP 471, Kasserine 1200
[*]Corresponding author: touaitibilel@gmail.com

***Abstract*—The rapid growth of electric scooters in urban environments requires efficient, reliable and user-friendly charging solutions for micromobility systems. Inductive power transfer (IPT) technology allows for contactless charging, reducing maintenance needs and improving operational safety. This paper presents the design and analysis of Series-Series (SS) compensated inductive power transfer converter (IPTC) for Electric Scooter charging applications. A systematic design methodology, based on analytical modeling and finite-element analysis, is developed to achieve efficient power transfer under practical operating conditions. The study investigates the effect of magnetic coupling and coil separation on voltage, current and power transfer efficiency by means of simulation and experimental validation on a laboratory scale prototype. The experimental results show a stable operation and a maximum power transfer efficiency of 93.5 % under nominal operating conditions and emphasize the effect of air-gap variation on the system performance. The proposed solution helps to develop a scalable, reliable and energy-efficient wireless charging infrastructure for sustainable electric scooter micromobility networks.**

Index Terms—Wireless Power Transfer, E-scooter, Inductive Power Transfer Converter (IPTC), Resonance Frequency, FEMM 4.2.

I. Introduction

Electric micromobility, especially electric scooters, has emerged as a promising solution for short-distance urban transport. However, conventional plug-in charging infrastructures present limitations related to user convenience, maintenance, connector degradation, and safety. To align micromobility systems with the long-term vision of sustainability, charging technologies must not only be efficient but also resilient, user-friendly, and adaptable to dense urban environments (Figure 1).

In consideration of these challenges, Wireless Power Transfer (WPT), specifically Inductive Power Transfer Converter (IPTC), has emerged as a viable alternative to electrical charging systems. IPTC systems utilize two linked coils operating within medium to high-frequency ranges, with resonant compensation networks to improve power transfer efficiency under inadequately coupled situations and varying air gaps [1-2]. The theoretical principles of resonant inductive coupling and efficiency optimization were first illustrated in strongly coupled magnetic resonance systems [3], while later studies developed systematic design approaches for compensation topologies and control strategies [4].

Among the earliest and most widely used compensation configurations is the Series–Series (S/S) topology. In this structure, both the primary and secondary sides are series compensated. At the resonant frequency, the load current becomes approximately constant, which facilitates stable power transfer and simplifies control strategies. Moreover, Zero Voltage Switching (ZVS) conditions can be achieved relatively easily, reducing switching losses and improving system efficiency. However, under weak magnetic coupling conditions, the S/S topology may lead to increased current levels when the load decreases, which can affect system stability and efficiency [5].

Another commonly investigated configuration is the Series–Parallel (S/P) compensation topology. This topology allows certain flexibility in the network design, making it suitable for dynamic wireless charging systems and applications requiring adaptive control. For instance, it has been proposed for wireless power transfer systems in which power outlets can be automatically activated through inductive coupling mechanisms [6-7]. One advantage of the S/P topology is its capability to deliver higher current levels relative to the coupling coefficient. Nevertheless, due to the presence of capacitive components in the reflected impedance, achieving ZVS operation becomes more difficult compared with the S/S configuration.

The Parallel–Series (P/S) topology has also been explored for IPTC, particularly in circuits with minimal inductance requirements. Although it offers certain design advantages, this topology introduces considerable voltage stress across switching devices and can result in significant variations in output power as the magnetic coupling coefficient changes. In addition, since the system operates as a current-source inverter, achieving ZVS conditions becomes more challenging [8].

To overcome the limitations of basic compensation structures, several advanced topologies have been proposed. The LCCL/S compensation topology maintains a constant transmitter current at the resonant frequency and enables effective filtering of transmitter current, which helps reduce power fluctuations during operation. This characteristic makes it attractive for wireless charging applications requiring stable power delivery. However, the main drawback of this configuration is the increased circuit complexity and the larger size and volume of the compensation components [9].

Similarly, the LCCL/P topology has been investigated for wireless power transfer systems. Although it maintains constant transmitter current at resonance, it exhibits larger power variations compared to the LCCL/S configuration. Moreover, because the reflected impedance contains capacitive elements, achieving ZVS operation becomes more difficult [10].

Further improvements in current control and filtering performance can be achieved using the LCCL/LCCL topology, which provides effective filtering of both transmitter and receiver currents while maintaining good control of the transmitter current. This topology reduces power variations caused by changes in the coupling coefficient. However, it requires larger compensation capacitors than simpler topologies, increasing the size and complexity of the system [11].

Overall, the selection of an appropriate compensation topology is a critical step in the design of high-performance IPTC. Factors such as power transfer efficiency, robustness against coupling variations, switching conditions, and circuit complexity must be carefully considered. In the context of electric scooter micromobility charging, these aspects become even more important due to the compact system size, variable alignment conditions, and efficiency requirements. Therefore, the design and optimization of an appropriate IPTC topology remain key challenges for improving the performance of wireless charging systems.

Despite the significant progress in compensation network design for wireless power transfer systems, challenges remain in achieving high efficiency, stable power delivery, and reduced sensitivity to misalignment in compact micromobility charging applications. In particular, electric scooter charging systems require optimized IPTCs capable of operating efficiently under static wireless charging conditions, where coil alignment variations and compact system dimensions can strongly affect magnetic coupling and power transfer performance.

In this paper, an efficiency IPTC is designed and optimized for static wireless charging of electric scooters. The proposed system focuses on improving magnetic coupling and overall power transfer efficiency through an optimized compensation network and coil design. A detailed analysis of the converter topology and system parameters is performed to enhance power transfer capability while ensuring stable operation and soft-switching conditions. Furthermore, the influence of key design parameters, including coupling coefficient, resonant components, and load conditions, is investigated to evaluate the performance of the proposed IPT system. The effectiveness of the proposed design is validated through simulation and experimental analysis, demonstrating its suitability for compact and efficient micromobility charging applications.

Figure 1 : Conceptual image of the integration of renewable energy generation for E-scooters wireless charging infrastructure

II. CIRCUIT CONFIGURATION AND ANALYSIS OF THE IPTC

The proposed topology of IPTC for contact free charging of electric scooters is shown in Fig. 2. The IPTC comprises of a grid-side power conversion stage, a magnetically coupled resonant interface and a vehicle-side power conditioning stage. The main side is converted from low-voltage AC to regulated DC bus by AC–DC rectifier and DC-link capacitor. The excitation is sinusoidal or quasi-sinusoidal and is generated by a high-frequency Voltage-Source Inverter (VSI). This excitation is fed into the main resonant tank, which is the transmitter inductance and compensating capacitor.

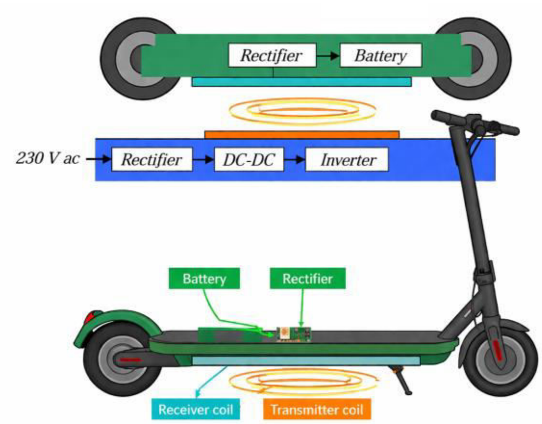

Fig. 2. Configuration of the E-scooters wireless charging system.

Figure 3 illustrates the geometric configuration of the inductive coupling interface used in the proposed IPTC. The structure consists of two planar rectangular coils arranged in a coaxial and vertically separated alignment. The primary (transmitting) coil, defined by dimensions a1 and b1, is positioned on the lower side, while the secondary (receiving) coil, characterized by dimensions a2 and b2, is placed above it. The separation distance d represents the air gap between the coils, which plays a critical role in determining the magnetic coupling strength. This simplified geometry is adopted to facilitate accurate electromagnetic modeling while preserving the key physical parameters governing power transfer. In particular, the coil dimensions and the inter-coil d directly influence the mutual inductance and coupling coefficient, thereby affecting the overall efficiency and power transfer capability of the system.

the values of R_i and L_i can be calculated as follows:

$$R_i = N_i.\rho\frac{2(a_i+b_i)}{S_i} \quad (1)$$

$$L_i = \frac{\mu_0}{\pi}N_i^2\left[a_i.\ln\frac{2a_ib_i}{r_i(a_i+\beta)} + b_i.\ln\frac{2a_ib_i}{r_i(b_i+\beta)} - 2(\alpha-\beta) + 0.25\alpha\right] \quad (2)$$

Where: N_i is number of turns, $\alpha = a_i + b_i$, $\beta = (a_i^2 + b_i^2)^{0.5}$, In equations (1) and (2), i=p denotes the primary coil, while i=s represents the reception coil. Given that the primary coil is significantly longer than the reception coil (b1>>b2), the mutual inductance M can be computed analytically as follows:

$$M = \frac{\mu_0}{\pi}N_1N_2b_2\ln\left[\frac{\sqrt{d^2+a_1^2}}{d}\right] \quad (3)$$

Where: N_1 and N_2 are number turns of the transmitter and receiver coils respectively; d is the air gap (distance between the transmitter and receiver coils); μ_0 is the permeability of vacuum ($\mu_0 = 4\pi \times 10^{-7}$); b_2 is the length of the receiver coil; a_1 width of the transmitter coil.

Overall, the expression highlights that mutual inductance increases with coil size and number of turns, and decreases as the air gap between the coils becomes larger. These parameters are critical in determining the efficiency of inductive power transfer systems.
The coupling coefficient (k) and mutual inductance (M) are expressed as follows.:

$$k = \frac{M}{\sqrt{L_p * L_s}} \quad (4)$$

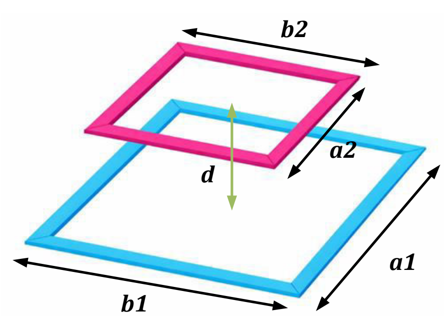

Fig. 3. Rectangular coils design

Figure 4 shows that he mutual inductance decreases nonlinearly with the increase in separation distance. A strong magnetic coupling is observed at short distances, while the coupling gradually weakens as the air gap increases, following a logarithmic-like decay behavior.

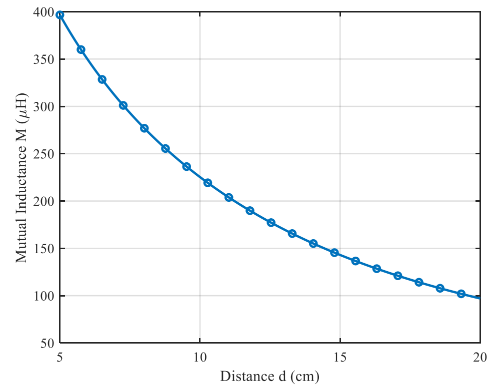

Fig .4. Effect of air gap distance on the mutual inductance.

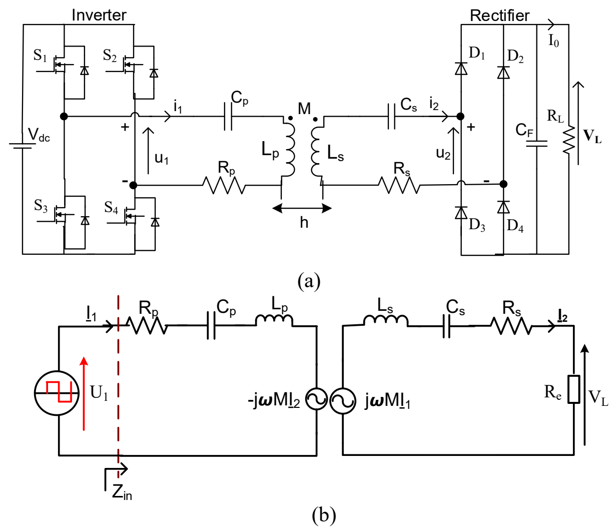

Fig .5. Electrical Circuit Equivalent for IPTC.

The corresponding equation system at both primary and secondary circuit sides can be expressed as:

$$\begin{cases} \underline{V_1} = (R_p + j\omega_S L_p + \frac{1}{j\omega_S C_p})\underline{I_1} - j\omega_S M\underline{I_2} \\ j\omega_S M\underline{I_1} = (R_s + j\omega_S L_s)\underline{I_2} + Z_2\underline{I_2} \end{cases} \quad (5)$$

As illustrated in Fig. 5, The secondary series impedance Z_2 can be determined as following:

$$Z_2 = R_e + \frac{1}{j\omega_S C_s} \quad (6)$$

The electrical behavior of the inductive power transfer system is modeled using the equivalent impedances of the primary and secondary resonant circuits. The primary-side impedance Zp is expressed as:

$$Z_p = R_p + j\omega_s L_p + \frac{1}{j\omega_S C_p} \quad (7)$$

The last expression captures both the resistive losses and the reactive behavior of the series-compensated primary resonant tank.

Similarly, the total impedance of the secondary side is given by:

$$Z_s = R_s + j\omega_s L_s + Z_2 \quad (8)$$

Based on the coupled-circuit model, the primary current I_1 can be derived as:

$$\underline{I_1} = \frac{V_1}{Z_p + (\omega_S M)^2 / Z_s} \quad (9)$$

The term $\frac{(\omega_S M)^2}{Z_s}$ represents the reflected impedance of the secondary circuit onto the primary side, highlighting the strong dependency of the primary current on the coupling condition and load characteristics.
The secondary current I_2 is then obtained from the mutual coupling relationship as:

$$\underline{I_2} = \frac{j\omega_S M}{Z_s} \underline{I_1} \quad (10)$$

The last expression shows that the secondary current is directly proportional to the mutual inductance and the primary current, and inversely proportional to the total secondary impedance. This formulation clearly illustrates the impact of coupling strength and secondary-side loading on the power transfer capability of the IPTC.

The complex input impedance of the IPTC, as seen from the primary source, equation 11, is given by Zin,ss. It consists of the primary compensated impedance and the reflected secondary impedance through magnetic coupling. The term $j\left(\omega_s L_p - \frac{1}{\omega_s C_p}\right)$ represents the net reactive component of the primary resonant tank, while the fraction $\frac{\omega_s{}^2 M^2}{R_s + R_e + j(\omega_s L_s - \frac{1}{\omega_s C_s})}$ denotes the reflected impedance of the receiver-side compensated network and load. This expression highlights the dependence of the source-side impedance on coupling strength, compensation design, and load conditions in steady-state operation.

$$Z_{in\_SS} = R_p + j\left(\omega_s L_p - \frac{1}{\omega_s C_p}\right) + \frac{\omega_s{}^2 M^2}{R_s + R_e + j(\omega_s L_s - \frac{1}{\omega_s C_s})} \quad (11)$$

The efficiency η of the IPTC is defined as the ratio of the power delivered to the load P_L to the total input power P_{in}. As shown in the equation, the output power is expressed as **[5]**:

$$P_L = R_e I_0^2 \quad (12)$$

where I_0 is the load current and R_e is the equivalent resistive load. The total power losses in the system consist of the conduction losses in the primary coil $R_p I_1^2$, the secondary coil $R_s I_2^2$, and the power dissipated in the load. Thus, the efficiency is given by **[10]**:

$$\eta = \frac{P_L}{P_{in}} = \frac{R_e I_0{}^2}{R_p I_1{}^2 + R_s I_2{}^2 + R_e I_0{}^2} \quad (13)$$

For a normalized form, the equation can be rewritten as:

$$\eta = \frac{R_e}{R_p(\frac{I_1}{I_0})^2 + R_s(\frac{I_2}{I_0})^2 + R_e} \quad (14)$$

This formulation highlights how the efficiency depends not only on the load resistance Re, but also on the current ratios I_1/I_0 and I_2/I_0, which are determined by the magnetic coupling, compensation topology, and operating frequency. A higher efficiency is achieved when the power losses in the primary and secondary coils are minimized relative to the power delivered to the load.
As illustrated in Figure 4, for the SS compensation, the receiver coil current is same that the load current ($i_2 = i_0$). Substituting the secondary current, I2 in Eq. (10) into Eq. (14), the efficiency of SS topology can be expressed as following:

$$\eta = \frac{R_e}{R_p[\frac{Z_S}{\omega_S M}]^2 + R_s + R_e} = \frac{\omega_S{}^2 M^2 R_e}{R_p[(R_s + R_e)^2 + X_s{}^2] + (R_s + R_e)\omega_S{}^2 M^2} \quad (15)$$

Where: $X_s = \omega_s L_s - \frac{1}{\omega_s C_s}$ the equivalent reactance of receiver circuit Xs.
In resonance conditions inside a SS compensated IPTC circuit, the reactive impedance components of both the primary and secondary circuits are eliminated by the series capacitive compensation. The relationships between voltage and current are exclusively determined by the resistive and mutual inductive elements. At resonance, the current in the secondary coil I_2 equals the load current I_0. By putting this into the general equation for efficiency and simplifying, the power transfer efficiency η may be calculated as follows:

$$\eta = \frac{\omega_0{}^2 M^2 R_e}{R_p(R_s + R_e)^2 + \omega_0{}^2 M^2 (R_s + R_e)} \quad (16)$$

Where: $\omega_0 = 2\pi f_0$

As illustrated in Figure 6, the power transfer efficiency increases with the coupling coefficient k, which emphasizes the role of magnetic coupling in enhancing the energy transfer between the primary and secondary coils. The maximum efficiency increases from less than 10% for k=0.01 to about 90% for k=0.10, still centered around the resonant frequency of 10 kHz. In the investigated coupling range, the system shows one dominant resonance peak, which means that the critical coupling threshold related to the frequency splitting has not been reached. This behavior indicates stronger electromagnetic interaction but also greater sensitivity to tuning. The results highlight that increasing k enhances efficiency but introduces dual resonances and potential impedance mismatch; thus, optimal operation occurs just below the onset of mode splitting, ensuring high efficiency and stable frequency performance.

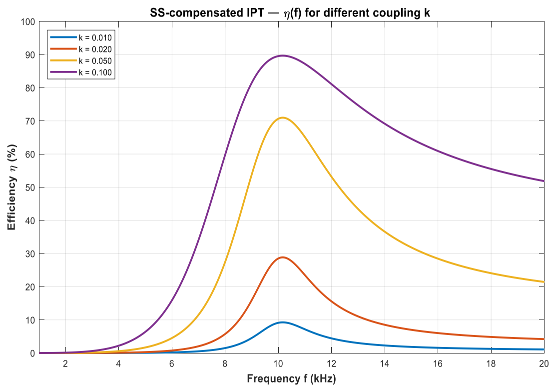

Figure 6: Efficiency η vs. Frequency for different coefficient coupling k.

III. System Simulation

In this section, the finite-element evaluation of the proposed IPTC with FEMM 4.2 is presented to characterize the magnetic coupling between the transmitter and receiver coils and extract the self- and mutual inductances. The analysis was carried out according to the design specifications in the Table I. The model has 1660 mesh elements and a coil separation of 150 mm. It can be observed that the magnetic flux is mainly concentrated in the coupling region with limited leakage flux in the surrounding air under nominal operating conditions. The symmetric flux distribution confirms the proper alignment of the coils and the lack of localized flux concentration indicates the appropriate coil geometry for the desired wireless power transfer operation.

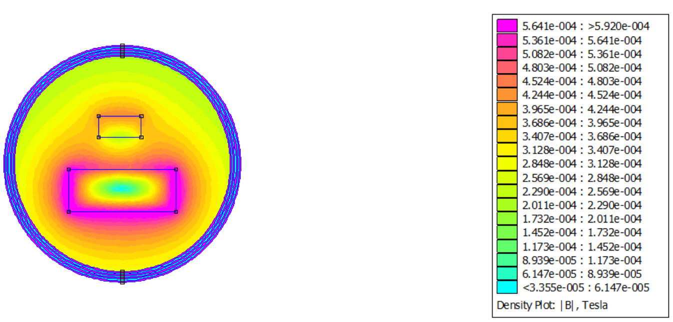

Figure 7: Magnetic flux density distribution |B|, (T) of the IPTC coils for e-scooter wireless battery charging, obtained using FEMM 4.2

IV. Experimental Validation

The experimental setup is illustrated in Fig. 8. It comprises four principal units: a DC power supply, a DC–AC inverter implemented with four IGBT switches, an inductive coupling system formed by two rectangular coils, and a rectification stage supplying a resistive load. The main design and operating parameters of the developed prototype are reported in Table II.

To mitigate additional losses caused by skin and proximity effects, both coils are fabricated using Litz wire with a cross-sectional area of 1.5 mm². The equivalent radii of the primary and secondary coils are estimated to be r1=5.8 mm and r2=6.9 mm, respectively, as depicted in Fig. 2. The inverter switching signals are produced using a dSPACE DS1104 control board, enabling accurate control of the converter operation.

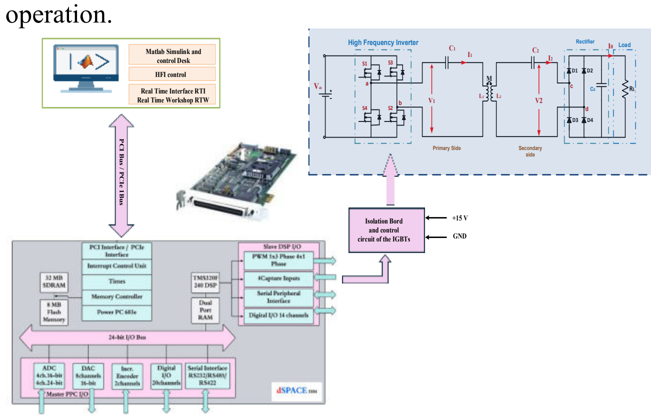

Fig. 8. Experiment setup of the proposed wireless charging system

Table I summarizes the nominal parameters of the proposed inductive power transfer system. The system is supplied by a 120 V DC source and delivers power to a 45 Ω load.

TABLE I : Nominal Parameters of the Proposed IPTC

Category	Parameter	Symbol	Value
Geometry	Transmitter coil dimensions	a1 × b1	0.2 m × 0.5 m
	Receiver coil dimensions	a2 × b2	0.2 m × 0.1 m
Windings	Number of turns (Tx / Rx)	N1, N2	70 / 100
Electrical	Coil resistances (Tx / Rx)	R1, R2	1.15 Ω / 0.78 Ω
	Self-inductances (Tx / Rx)	L1, L2	4.7 mH / 2.9 mH
Compensation	Capacitors (Tx / Rx)	C1, C2	55 nF / 88 nF
Operation	Switching frequency	fs	10 kHz
	DC input voltage	Vdc	120 V
Load	Load resistance	RL	45 Ω

Figure 9 shows the experimental voltage and current waveforms of the compensated inductive power transfer system for two air-gap distances: 10 cm and 15 cm. Primary and secondary voltages are shown in (a) and (b), while corresponding currents are shown in (c) and (d).

Figure 9 summarizes the experimental quantitative and qualitative evaluation of system performance over different transfer lengths. The experimental prototype was an SS compensated IPTC with a resonant frequency of 10 kHz and a primary voltage of 120 V. At the nominal operating condition, i.e., for a 10 cm air gap, the measured secondary voltage and RMS current were 96 V and 3.34 A. As the magnetic coupling between the transmitter and receiver coils decreased, the air gap was increased to 15 cm, resulting in a reduction of the secondary voltage to 63 V and the RMS current to 1.46 A. These results show the strong dependence of the power transfer performance on the coil separation, and stable resonant operation under different air-gap conditions.

The phase shift observed between the primary and secondary voltages in Fig. 9 is mainly due to the magnetic coupling between the coils and the phase response of the SS-compensated resonant network. The mutual inductive coupling and the reflected impedance from the secondary side together create a phase displacement between V_p and V_s when the system is near its resonant frequency. Other contributions from component tolerances and parasitic elements may additionally alter the measured phase relation.

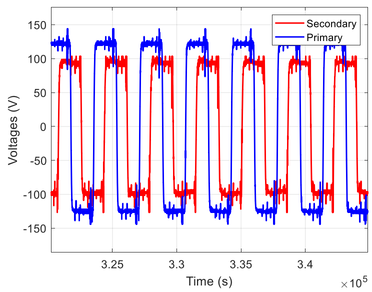

(a)
Vp = 120V ; Vs = 96V pour 10 cm

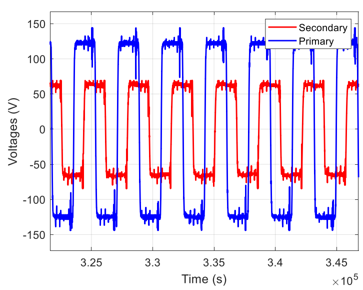

(b)
Vp = 120V ; Vs = 63V pour 15 cm

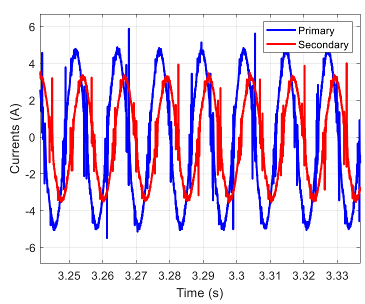

(c)
Ip (eff) = 3.4A ; Is (eff) = 2.34A pour 10 cm

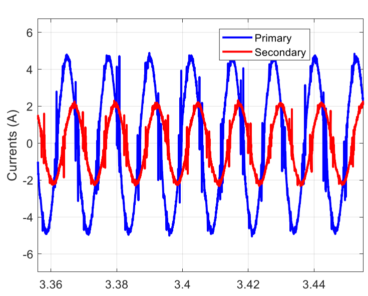

(d)
Ip (eff) = 3.4A ; Is (eff) = 1.46A pour 15 cm

Fig. 9. Experiment result of the proposed IPTC

V. Conclusion

this paper, the design and experimental verification of series-series (SS) compensated inductive power transfer converter (IPTC) for electric scooter wireless charging is presented. The coil topology was chosen to be rectangular for better magnetic coupling stability for both aligned and misaligned cases. The proposed design was validated by finite-element simulations and a 10 kHz prototype. The results showed maximum coil-to-coil efficiency of 93.5% at the nominal operating conditions. Experimental tests demonstrated that the increase of the air gap resulted in a reduction of magnetic coupling and in a reduction of the secondary voltage and current. The tested range was characterized by stable resonant operation. The good agreement between simulation and experimental results confirms the proposed design methodology for micromobility wireless charging applications. Future work will focus on higher power implementations, electric vehicle charging applications, and studies of thermal behavior, electromagnetic compatibility and advanced compensation and control techniques.

References

[1] D. Hung Tran, V. Binh Vu, and W. Choi, “High-Efficiency Wireless Power Transfer System With Intermediate Coils for the On-Board Chargers of Electric Vehicles,” *IEEE Transactions on Power Electronics,* vol. 33, n. 1, pp. 1044 – 1058, January 2018.

[2] Hong Zhou, Bin Zhu, Wenshan Hu, Zhiwei Liu, and Xingran Gao, “Modelling and Practical Implementation of 2-Coil Wireless Power Transfer Systems,’’ *Journal of Electrical and Computer Engineering*, vol. 1, no.9, pp. 1 - 9, Sep. 2014.

[3] H. Yao-Ching; Zhong-Rong Lin ; Ming-Cheng Chen ; Hsin-Che Hsieh ; Yu-Chen Liu ; Huang-Jen Chiu, , “ High-Efficiency Wireless Power Transfer System for Electric Vehicle Applications,’’ *IEEE Transactions on Circuits and Systems II: Express Briefs*, Vol. 64, no.8,pp. 942 - 946, Aug. 2017.

[4] S.D. Barman, A.W. Reza, N. Kumar, Md.E. Karim, A.B. Munir, Wireless powering by magnetic resonant coupling: Recent trends in wireless power transfer system and its applications, *Renewable and Sustainable Energy Reviews*, vol. 51, n. 1, pp. 1525–1552, Nov. 2015.

[5] C. Park, S. Lee, S. Y. Jeong, G.-H. Cho, and C. T. Rim, ‘‘Uniform power I-type inductive power transfer system with DQ-power supply rails for on-line electric vehicles,’’ *IEEE Trans. Power Electron.,* vol. 30, no. 11, pp. 6446–6455, Nov. 2015,

[6] J. M. Miller, O. C. Onar, and M. Chinthavali, ‘‘Primary-side power flow control of wireless power transfer for electric vehicle charging,’’ *IEEE J. Emerg.Sel. Topics PowerElectron*., vol. 3, no. 1, pp. 147–162,Mar.2015.

[7] J. Sallán, J. L. Villa, A. Llombart, and J. F. Sanz, ‘‘Optimal design of ICPT systems applied to electric vehicle battery charge,’’ *IEEE Trans. Ind. Electron.,* vol. 56, no. 6, pp. 2140–2149, Jun. 2009,

[8] R. Singh, P. Sanjeevikumar, D. S. Kumar, M. Molinas, and F. Blaabjerg, Eds., Cable Based and Wireless Charging Systems for Electric Vehi cles: Technology and Control, Management and Grid Integration. Edison, NJ, USA: Institution of Engineering and Technology, 2021,

[9] G. R. Nagendra, G. A. Covic, and J. T. Boys, ‘‘Sizing of inductive power pads for dynamic charging of EVs on IPT highways,’’ *IEEE Trans. Transport. Electrific.,* vol. 3, no. 2, pp. 405–417, Jun. 2017,

[10] H. Feng, T. Cai, S. Duan, J. Zhao, X. Zhang, and C. Chen, ‘‘An LCC compensated resonant converter optimized for robust reaction to large coupling variation in dynamic wireless power transfer,’’ *IEEE Trans. Ind. Electron.,* vol. 63, no. 10, pp. 6591–6601, Oct. 2016

[11] F. Lu, H. Zhang, H. Hofmann, and C. C. Mi, ‘‘A dynamic charging system with reduced output power pulsation for electric vehicles,’’ *IEEE Trans. Ind. Electron.,* vol. 63, no. 10, pp. 6580–6590, Oct. 2016, doi: 10.1109/TIE.2016.2563380.